High Power Laser Science and Engineering, (2025), Vol. 13, e21, 8 pages.
doi:10.1017/hpl.2025.10

HIGH POWER LASER SCIENCE AND ENGINEERING

RESEARCH ARTICLE

Focal spot polarization distribution under polarization smoothing

Yanghui Tang[1,2], Shenlei Zhou[1], Shouying Xu[1], and Cheng Liu[1]

[1] *Key Laboratory of High Power Laser and Physics, Shanghai Institute of Optics and Fine Mechanics, Chinese Academy of Sciences, Shanghai, China*

[2] *Center of Materials Science and Optoelectronics Engineering, University of Chinese Academy of Sciences, Beijing, China*

(Received 15 November 2024; revised 24 December 2024; accepted 14 January 2025)

Abstract

Polarization smoothing can effectively improve the uniformity of focal spots. In this study, we theoretically and experimentally investigated the polarization synthesis of the focal spot under a birefringent wedge (BW) and speckle under the coupling of the BW and continuous phase plate. Polarization distribution was experimentally obtained using rotating quarter-wave plate measurement under a specific wedge angle. The simulated and experimental results are consistent, demonstrating that the focal spot is in a state of coexistence of elliptical and linear polarizations. In addition, the polarization state is determined by the ratio of the amplitudes and the phase difference between the sub-beams. The simulation results showed that the proportion of linear polarization increased with the separation angle of the sub-beam. In contrast, it decreased with the incident light aperture. This research is crucial for accurately describing the polarization distribution and further understanding the laser–plasma interactions.

Keywords: polarization smoothing; polarization synthesis; Stokes parameters

1. Introduction

Inertial confinement fusion (ICF) with direct or indirect drive requires highly uniform focus spot intensity that is illuminated to the target to reduce low-mode inhomogeneity and laser–plasma instabilities (LPIs)[1–4]. A variety of large-scale laser driving systems currently tend to employ the continuous phase plate (CPP), smoothing by spectral dispersion (SSD) and polarization smoothing (PS) to achieve beam smoothing[5–9]. The CPP is a spatial smoothing method that modulates the near-field phase wavefront to obtain the required focal spot envelope; SSD reduces the coherence in time to reduce or even eliminate laser speckles under time integration; and PS divides the beam into two orthogonally polarized beams through a birefringent crystal to guarantee the incoherent superposition of far-field focal spots and reduce the contrast of focal spot intensity[10–14].

PS can effectively suppress plasma filamentation because of its instantaneous smoothness[6]. Many studies have been conducted on various birefringent components that realize PS, including liquid crystal, deuterated potassium dihydrogen phosphate (DKDP) and potassium dihydrogen phosphate (KDP)[15–19]. These findings demonstrate that focus spot uniformity can be enhanced, and the LPI can be suppressed by combining these birefringent materials with the CPP and SSD[5,11,13]. The reduction of the intensity contrast was the primary objective of the PS-obtained focal spot in previous research. Recent studies, however, show that distinct LPI processes are suppressed differently by various polarization states[20,21]. As an example, stimulated Raman scattering (SRS) can be efficiently reduced by linear polarization, but the measurement results from the direct-drive experiment showed that linear polarization resulted in nonuniform cross-beam energy transfer (CBET) coupling between the beams[21,22]. CBET can disrupt energy coupling, reduce the ablation pressure and finely tune the symmetry of the laser drive[23,24]. Therefore, it is essential to study the polarization state of the focal spot under PS and accurately describe the polarization distribution.

Because the focal spots of ordinary and extraordinary rays are focused on the same far-field plane using the birefringence wedge, the ordinary ray is polarized perpendicular to the extraordinary light, and phase difference between the two orthogonal polarizations is introduced by PS and the CPP, which causes the final polarization distribution in the focal spot to present a state of staggered coexistence of

Correspondence to: S. Zhou, Key Laboratory of High Power Laser and Physics, Shanghai Institute of Optics and Fine Mechanics, Chinese Academy of Sciences, Shanghai 201800, China. Email: slzhou@siom.ac.cn

multiple polarization states. In this study, we built a far-field transmission model of the light field for a birefringent wedge (BW) and CPP, theoretically analyzed the beam splitting and polarization synthesis and applied Stokes parameters to calculate the azimuth and ellipticity of the polarization state in the focal spot. The effects of different separation angles between the ordinary and extraordinary parts on the polarization synthesis of the overlapping and nonoverlapping regions of the far-field sub-focal spot were further studied. Correspondingly, the rotation quarter-wave plate method was used to measure the internal polarization state for PS and a CPP combined with PS. In addition, the polarization distribution of the far-field focal spot under a large beam aperture was analyzed based on the parameters of the high-power laser system during operation.

2. Description of the polarization smoothing and Stokes parameters

PS uses a birefringent crystal to split an initial linearly polarized beam into two orthogonally polarized beams. These beams subsequently superimpose in the far field after passing through the lens, thereby reducing the far-field intensity modulation. There are two primary PS application schemes for high-power laser devices. One option is for National Ignition Facility (NIF) with indirect drive to incorporate tilted KDP plates in the converging light[12]. The other option is for the OMEGA scheme with direct drive, adding a BW in the parallel beam, as shown in Figure 1. The sub-focal spot partially overlaps in the far field due to the angular difference between the ordinary and extraordinary light in both schemes. The phase difference $\Delta\varphi$ causes the polarization distribution to be more complex after polarization synthesis in the far field.

The OMEGA device scheme was used as an example to analyze the far-field polarization synthesis. Owing to the angular difference, the phases in the CPP and optical paths in the birefringent crystals of ordinary and extraordinary beams converging at the same location differ. Consequently, the light fields of the two orthogonal beams in the focal plane are as follows:

$$E_{\mathrm{ffo}} = F\left\{\frac{1}{\sqrt{2}}E_{\mathrm{in}}\exp\left[i\varphi_{\mathrm{CPP}}(x,y)+i\varphi_{\mathrm{BW_o}}(x,y)\right]\right\},$$
$$E_{\mathrm{ffe}} = F\left\{\frac{1}{\sqrt{2}}E_{\mathrm{in}}\exp\left[i\varphi_{\mathrm{CPP}}(x,y)+i\varphi_{\mathrm{BW_e}}(x,y)\right]\right\}, \quad (1)$$

where $\varphi_{\mathrm{CPP}}(x,y)$, $\varphi_{\mathrm{BW_o}}(x,y)$ and $\varphi_{\mathrm{BW_e}}(x,y)$ are the phases introduced by the CPP and ordinary and extraordinary light introduced after the BW, respectively. Distinct polarization distributions were created when two orthogonal polarizations with different phase information were synthesized at the same location on the focal plane.

The Poincaré sphere, Jones vectors and Stokes parameters are frequently used to characterize polarization states[25]. The Stokes parameters, for which all measurement parameters are intensity parameters, are a reasonably convenient way to detect the polarization state because it is easy to measure the optical beam intensity and comparatively difficult to measure the phase information. In addition, the Stokes parameters can be used to represent unpolarized, partially polarized and completely polarized beams, which can meet the requirements of the characterization of multiple polarization states of the far-field focal spot under different experimental conditions. The Stokes parameters for the monochromatic light are expressed as follows[26]:

$$S = \begin{bmatrix} S_0 \\ S_1 \\ S_2 \\ S_3 \end{bmatrix} = \begin{bmatrix} E_x^2 + E_y^2 \\ E_x^2 - E_y^2 \\ 2E_xE_y\cos\varphi \\ 2E_xE_y\sin\varphi \end{bmatrix}, \quad (2)$$

in which E_x and E_y are the horizontal and vertical components of the light field, respectively, φ is the phase difference between the horizontal and vertical components, E_x and E_y represent ordinary and extraordinary light with vertical polarization, respectively, S_0 describes the optical field's total intensity, S_1 represents the excess of linearly

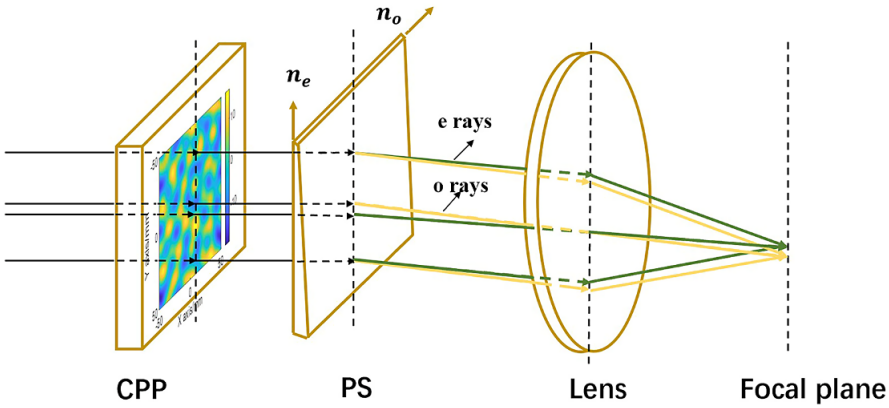

Figure 1. Schematic showing the use of a BW to achieve PS in the OMEGA scheme.

horizontally polarized light over linearly vertically polarized light and S_2 is $+45°$ linearly polarized light minus $-45°$ linearly polarized light. The last parameter, S_3, quantifies the preponderance of right-handed circularly polarized light over left-handed circularly polarized light[27]. The above far-field Stokes parameters can be obtained by Equation (1).

The Stokes parameters were measured using the rotating quarter-wave plate method, and the far-field polarization state of the incident beam smoothed by the CPP and PS was obtained. When this approach detects the Stokes parameters, the intensity $I(\theta)$ can be obtained using the Mueller formula after the incident light is transmitted through a quarter-wave plate rotating to a series of angles θ and a fixed horizontal linear polarization[27]:

$$I(\theta) = \frac{1}{2}\left(S_0 + S_1\cos^2 2\theta + S_2 \sin 2\theta \cos 2\theta + S_3 \sin 2\theta\right). \tag{3}$$

Equation (3) can be rewritten by using the trigonometric half-angle formula to yield the following:

$$I(\theta) = \frac{1}{2}\left(A + B\sin 2\theta + C\cos 4\theta + D\sin 4\theta\right). \tag{4}$$

Equation (4) is a part of the Fourier series, and the highest-frequency component is $4\theta\,(\theta = 2\pi ft)$. When measuring the polarization distribution in the far field, the minimum number of sampling points required is eight, according to Nyquist's sampling theorem, which states that the sampling rate must be at least twice that of the highest-frequency component to reconstruct the signal. Here, A, B, C and D were determined by calculating the coefficients of each harmonic component of the Fourier series. The Stokes parameters in Equation (3) are as follows[27]:

$$\begin{aligned} S_0 = A - C &= \frac{2}{N}\sum_{n=1}^{N} I_n - \frac{4}{N}\sum_{n=1}^{N} I_n \cos 4\theta_n, \\ S_1 = 2C &= \frac{8}{N}\sum_{n=1}^{N} I_n \cos 4\theta_n, \\ S_2 = 2D &= \frac{8}{N}\sum_{n=1}^{N} I_n \sin 4\theta_n, \\ S_3 = B &= \frac{4}{N}\sum_{n=1}^{N} I_n \sin 2\theta_n. \end{aligned} \tag{5}$$

The ellipse shown in Figure 2 is a graphical representation of the polarization state; amplitude ratios and phase differences determine its various orientations and shapes, and the ellipticity angle ψ and orientation angle χ can be used to characterize the polarization ellipse. These angles can be determined by the four Stokes parameters and are given by the following:

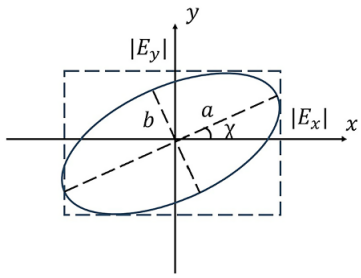

Figure 2. Polarization ellipse.

$$\tan 2\psi = \frac{S_3}{\sqrt{S_1^2 + S_2^2}} \quad (-45° \leqslant \psi \leqslant 45°), \tag{6}$$

$$\chi = \frac{1}{2}\arctan\left(\frac{S_2}{S_1}\right) \quad (0° \leq \chi \leq 180°). \tag{7}$$

Polarization synthesis is linearly polarized when the phase difference between E_x and E_y is $\varphi = m\pi$ $(m = 0, \pm 1, \pm 2, \cdots)$. When the amplitudes of E_x and E_y were equal and the phase difference was $\varphi = m\pi/2$ $(m = \pm 1, \pm 3, \pm 5\ldots)$, the synthesized polarization states were left- or right-handed circularly polarized light with $\psi = -45°$ and $45°$, respectively. In addition to the aforementioned special cases, the synthesized polarization state is an elliptical polarization[28].

3. Simulations and analysis

The BW causes a relative deflection between the ordinary and extraordinary components, resulting in spatially separated focal spots in the far-field plane. The wedge angle affects the focal spot size, energy and phase distribution in the overlapping region. As shown in Figure 3, we simulated the polarization distribution in the focal spots when the separation angles between the sub-focal spots were α = DL, 2DL, 5DL. Here, DL represents the diffraction limit $1.22\frac{\lambda}{D}$, which results from the physical limitations of focusing light through a lens system as well as the wave nature of light, where λ is the wavelength and D is the beam aperture. The ratio of ordinary to extraordinary light energy was set to 1:1 because the optimum beam smoothing effect was produced. The contrast of the focal spot intensity was reduced to 70% when the energies of ordinary and extraordinary light were equal[7]. Moreover, the beam aperture D was restricted to 18 mm owing to the quarter-wave plate diameter used in the experiment. Figure 3(c) shows two separate sub-focal spots when the beam passed through the BW, shown in yellow and green, respectively. For a single sub-focal spot, most of the focal spot energy was concentrated in the Airy disk, and the focus intensity distribution followed the Bessel function, oscillating and reducing from the center to the edge. Areas

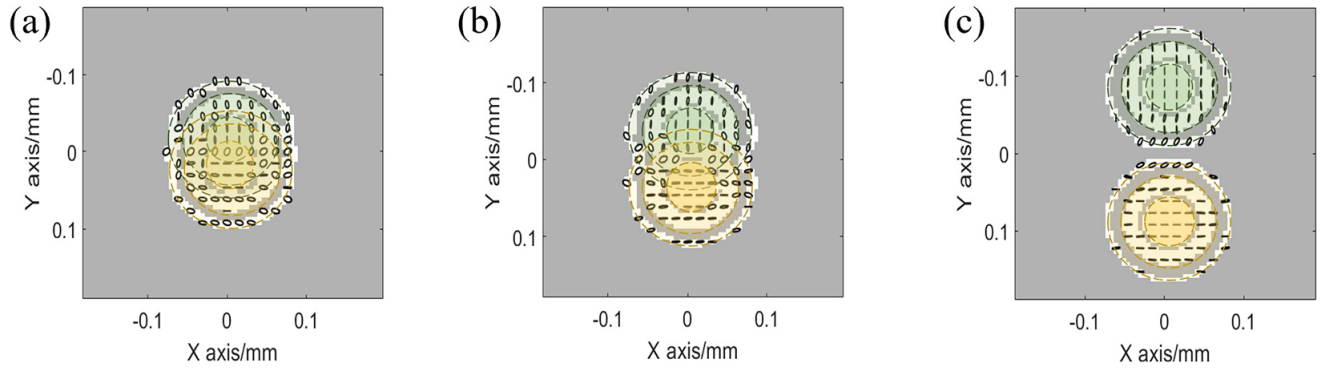

Figure 3. Polarization distribution within the focal point at various separation angles: (a) $\alpha = \mathrm{DL}$; (b) $\alpha = 2\mathrm{DL}$; (c) $\alpha = 5\mathrm{DL}$.

in the focal point, excluding the Airy disk, were defined as side lobes for the sake of description.

The analysis of Equation (2) reveals that when the amplitude difference between the two beams undergoing polarization synthesis is large, the synthesized polarization stays the same as the larger amplitude beam's polarization state. Conversely, when the amplitude difference of sub-beams is small, the synthesized polarization state varies with the amplitude ratio and phase difference between the two components. The polarization distribution when $\alpha = \mathrm{DL}$ is displayed in Figure 3(a). The two sub-focal spots are separated in the vertical direction and partially overlap. Since the central area of the Airy disk has the strongest amplitude, the other side that overlaps with a much smaller amplitude can be ignored in the calculation. The Stokes parameters at this position are $[1\ \ 1\ \ 0\ \ 0]^{\mathrm{T}}$ and $[1\ \ -1\ \ 0\ \ 0]^{\mathrm{T}}$, respectively, still horizontally or vertically linearly polarized. As there is a phase difference brought about by the BW and the amplitudes of the two orthogonal lights that overlap at the same place in other areas do not differ substantially, the elliptical polarization accounts for the majority of the polarization distribution. Figure 3(b) shows the polarization distribution under the separation angle $\alpha = 2\mathrm{DL}$. With the increase of the separation angle, the Airy disks in the two sub-focal spots are completely separated, leading to the polarization distribution here remaining essentially linearly polarized. The amplitude difference between the ordinary and extraordinary light converging at the same point increases. Thus, the polarization distribution in the side lobe either maintains linear polarization or is synthesized into elliptical polarization with different orientations and ellipticity angles. When the separation angle α is 5DL, the polarization synthesis is as shown in Figure 3(c). The side lobe amplitudes at the transverse tangent of the focus center are similar. As a result, the synthesized polarization at transverse tangent is elliptical polarization with different orientation angles, and the linear polarization in other areas remains unchanged due to the large amplitude difference.

In summary, elliptical polarization was generated when the amplitudes of the overlapping regions in the sub-focus were similar. However, linear polarization persisted when the amplitudes of the two were not of the same order of magnitude, even if the sub-focal spots overlapped. The linear polarization area in the focal spot increased and spread from the center of the Airy disks to the edge as the separation angle between the sub-focal spots increased.

Although PS can instantaneously smooth the focal spot, it has little effect on controlling the focal spot shape. With its ability to regulate the energy distribution and shape of the focal spot, the CPP is a phase-diffractive optical element that is frequently employed in conjunction with PS in high-power laser devices to smooth and shape beams. The beam that passes through the same position on the CPP is divided into two beams with separation angles after the BW, and these two beams no longer coincide at the same point on the focal plane. Nevertheless, ordinary and extraordinary light that converges at the same position on the focal plane for polarization synthesis passes through different microstructures of the CPP, and the CPP introduces different phase differences.

Figure 4 shows the polarization distribution of the far field when the CPP is combined with PS at different separation angles. Polarization synthesis involves linear polarization with a changing azimuth or elliptical polarization when the separation angle α between ordinary and extraordinary light is DL (Figure 4(a)). Elliptical polarization varies more in orientation and ellipticity than when only PS is applied. The amount of elliptical polarization at the edge of the focal spot decreased, and the linear polarization increased as the separation angle rose to two times the DL, as shown in Figure 4(b). When the separation angle is increased to five times the DL, the central region of the speckle is in a state of coexistence of elliptical and linear polarizations. The linear polarization region at the edge of the focal spot is further expanded (Figure 4(c)).

In conclusion, with the combination of the CPP and PS, polarization synthesis occurred throughout the focal spot when the separation angle of the sub-focal spot was DL. The center of the focal spots is still synthesized into various polarization states with an increase in the separation angle

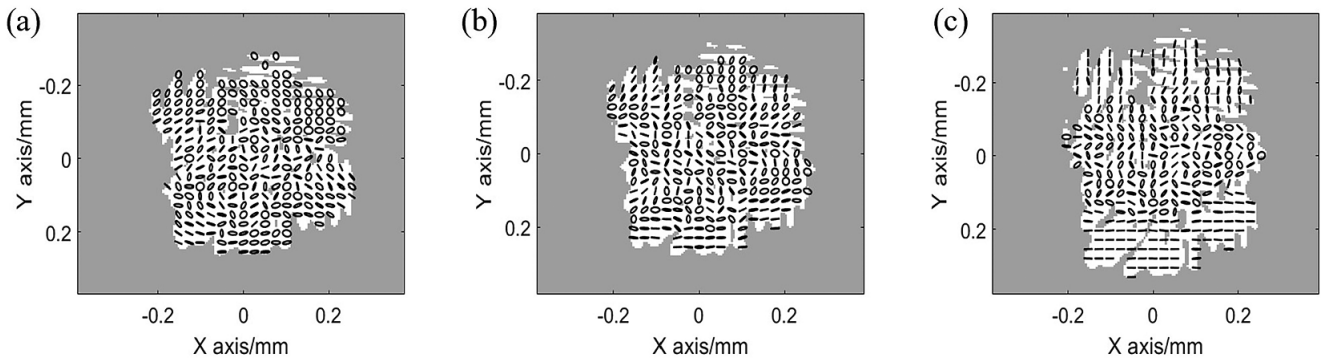

Figure 4. Polarization distribution of speckle when the CPP is combined with PS at different separation angles: (a) α = DL; (b) α = 2DL; (c) α = 5DL.

of the sub-focal speckles compared to PS alone, and linear polarization begins to appear at the edge speckle. The CPP introduces a continuous phase distribution, and the two orthogonal polarizations converge at the same point from the distinct positions of the CPP, resulting in a broader phase difference between the ordinary and extraordinary components. Because of this, the synthesized elliptical polarization has a distinct orientation and ellipticity angle, and it is more plentiful and diverse in the area where the sub-focal points overlap.

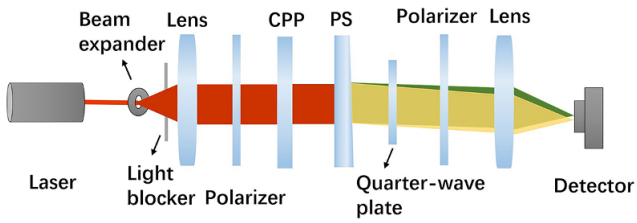

Figure 5. Setup to measure the polarization distribution in the far field using a rotating quarter-wave plate.

4. Experiments and discussion

The polarization states of the focal spot and speckle were acquired by rotating the quarter-wave plate in accordance with the Stokes parameter measurement method described in Section 2. Figure 5 shows the measurement configuration. The CPP and BW smoothed the 45° linearly polarized incident beam, and the energies of ordinary and extraordinary light were equal when the BW divided the beam into horizontal and vertical polarization states. The quarter-wave plate and fixed linear polarizer were positioned in front of the focusing lens in the parallel light because the quarter-wave plate is sensitive to the incident angle of the beam. The quarter-wave plate aperture was 18 mm, the initial direction of its fast axis was parallel to the horizontal direction, the polarizer's transmission axis was fixed horizontally and the detector gathered the focal spot focused by the lens. The Stokes parameters and distribution of the polarization state can be obtained by rotating the waveplate, measuring the focus spot intensity and applying Equation (5).

The focal point after the PS, spread on the 45° line, is shown in Figure 6(a) when the separation angle is 2DL. The wave plate's rotation angles are set to 0°, 18°, 36°, 54°, 72°, 90°, 108°, 126°, 144° and 162° for measurement precision. Figures 6(b) and 6(c) show the orientation and ellipticity angles of the elliptical polarization in the focal spot, respectively, as determined using Equations (6) and (7). As shown in Figure 6(b), the orientation angle of the polarization of the upper right sub-focal spot is approximately 90°, that is, the vertical direction; the orientation of the polarization at the lower left sub-focal spot is mostly 0° or 180°, that is, the horizontal direction. Figure 6(c) shows the ellipticity of polarization in the focal spot. The ellipticity of the overlapping area of the two sub-focal spots is approximately 40°, indicating elliptical polarization. Figure 6(d) shows the polarization distribution of the focus spot; the polarization state of the Airy disk remained either horizontally or vertically linear. Elliptical and linear polarizations are mutually doped in the side lobe with a lower intensity; in this case, the azimuth of the linear polarization differs, including both horizontal and vertical polarizations.

The nearly circular focal spot produced by combining the CPP and PS comprises many speckles (Figure 7(a)). Compared with Figure 6(b), various orientations mix with horizontal and vertical directions because of the addition of the CPP, as shown in Figure 7(b). In addition, as shown in Figure 7(c), the ellipticities of 0°, 45° and other angles are intermingled. The linear, circular and elliptical polarizations in the focal spot are mixed. The polarization distribution throughout the speckle is displayed in Figure 7(d). Linear polarization with different azimuths and elliptical polarization with varying orientations and ellipticities were the two forms of polarization observed in the speckles.

Different polarization states, including linear and elliptical polarization, may have varying inhibitory effects on various LPI processes in focal patterns. Some results have shown that there are overlapping regions in the path of transmission, resulting in multi-beam LPI, such as CBET[29]. When the incident beam is linearly polarized, the scattering level

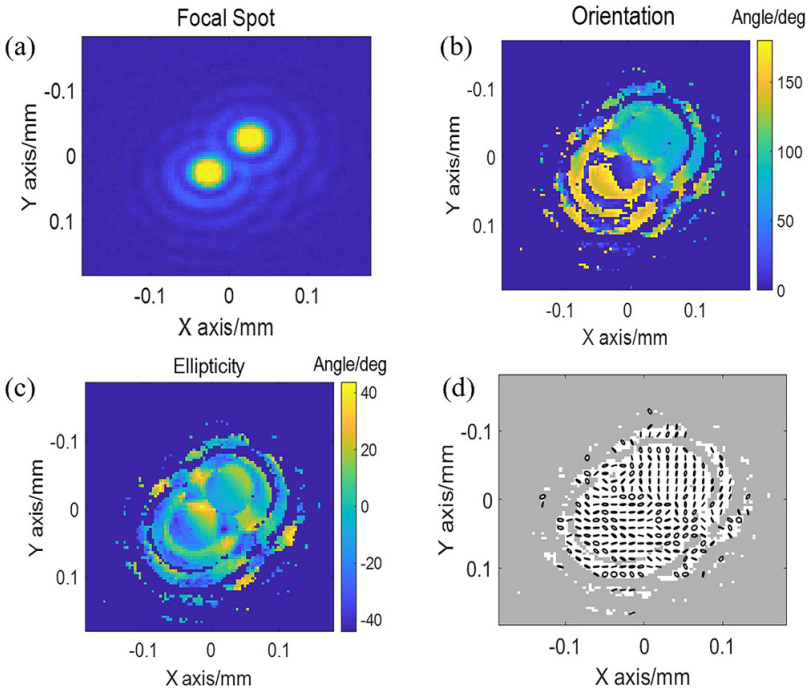

Figure 6. Focal spot after PS: (a) intensity distribution; (b) orientation of polarization calculated by Stokes parameters; (c) ellipticity; (d) polarization distribution.

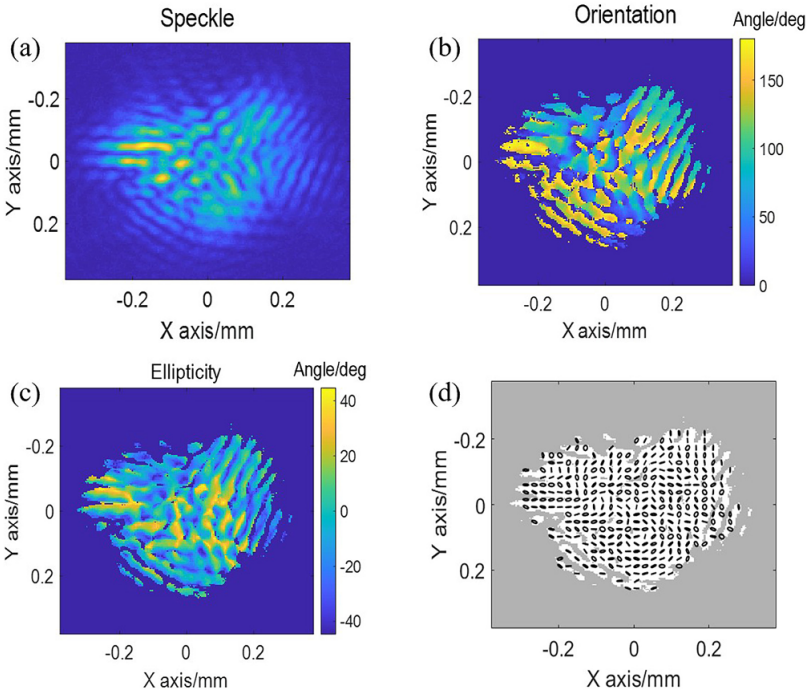

Figure 7. Speckle after the CPP and PS: (a) intensity distribution; (b) orientation; (c) ellipticity; (d) distribution of polarization states.

can be dramatically reduced, but the existence of linearly polarized regions will result in nonuniform CBET coupling between beams. In addition, if the proportion of various polarization states can be adjusted, the energy coupling efficiency and focal spot uniformity may be improved, which will suppress the instabilities such as LPI and Rayleigh–Taylor instability.

The aperture of the ICF laser driver in service is much larger than that used in this experiment; therefore, the far-field polarization distribution of the larger-aperture laser driver was simulated. The aperture of the CPP is 300 mm, the aperture of the incident beam is 280 mm, the diameter of the shaped speckle is 300 μm and the focal length of the lens is 1000 mm. Figures 8(a)–8(c) show the multiple

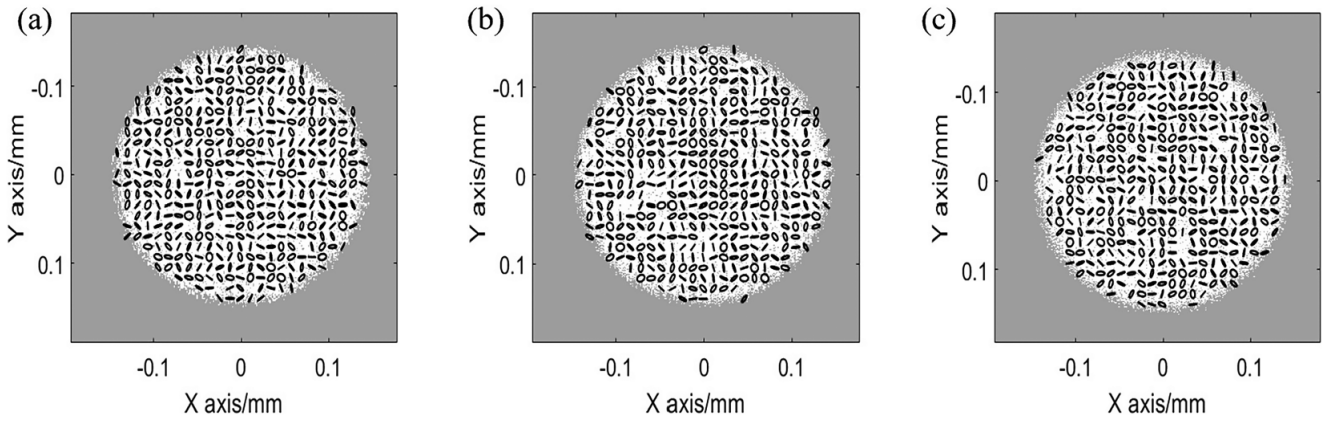

Figure 8. Simulation of far-field polarization distribution of the large-aperture laser driver at various separation angles: (a) DL; (b) 2DL; (c) 5DL.

polarization states of the speckle when the separation angles are DL, 2DL and 5DL. Because the DL decreases as the incident beam aperture increases and there is still significant overlap between the focal areas even when the separation angle is 5DL, the synthetic elliptical polarization in the speckle is further increased. The linear polarization at the edge is minimized compared to the polarization distribution with a small aperture. Under the above conditions, there is still a certain distribution of linearly polarized beams in the focal spot, and its proportion affects the final smoothing performance. However, the polarization distribution in the far field can theoretically be optimized by setting parameters of the CPP surface and the separation distance of the sub-focus, which requires further investigation.

5. Conclusion

In conclusion, we have demonstrated that the coexistence of distinct linear and elliptical polarizations with different orientations and ellipticities occurs in the focal spot. The polarization synthesis is determined by the ratio of the amplitudes and the phase difference between the sub-beams. In addition, the simulation results showed that as the separation angle between the sub-focal speckles rose, the proportion of linear polarization progressively increased, while elliptical polarization did the opposite. Further analysis was performed on the polarization distribution using a large beam aperture. The proportion of linear polarization at the edge of the focal spot decreases at the same separation angle because of the wider beam aperture. It is theoretically possible to optimize the CPP parameters to precisely regulate the distribution area and proportion of polarization states in the focused spot, hence improving the energy coupling efficiency and suppressing the LPI processes. These results have obvious important implications in the context of understanding the laser–plasma interaction.

Acknowledgements

This work was supported by the Strategic Priority Research Program of the Chinese Academy of Sciences (Grant No. XDA25020304) and the SG-II laser facility.

References

1. D. S. Montgomery, Phys. Plasmas **23**, 055601 (2016).
2. C. Zhang, C. Yu, C. Yang, D. Xiao, J. Liu, and Z. Fan, Phys. Plasmas **26**, 022707 (2019).
3. G. Cristoforetti, P. Koester, S. Atzeni, D. Batani, S. Fujioka, Y. Hironaka, S. Hüller, T. Idesaka, K. Katagiri, K. Kawasaki, R. Kodama, D. Mancelli, Ph. Nicolai, N. Ozaki, A. Schiavi, K. Shigemori, R. Takizawa, T. Tamagawa, D. Tanaka, A. Tentori, Y. Umeda, A. Yogo, and L. A. Gizzi, High Power Laser Sci. Eng. **11**, e24 (2023).
4. C. N. Danson and L. A. Gizzi, High Power Laser Sci. Eng. **11**, e40 (2023).
5. R. Zhang, H. Jia, X. Tian, H. Yuan, N. Zhu, J. Su, D. Hu, Q. Zhu, and W. Zheng, Opt. Lasers Eng. **85**, 38 (2016).
6. E. Lefebvre, R. L. Berger, A. B. Langdon, B. J. MacGowan, J. E. Rothenberg, and E. A. Williams, Phys. Plasmas **5**, 2701 (1998).
7. G. Miyaji, N. Miyanaga, S. Urushihara, K. Suzuki, S. Matsuoka, M. Nakatsuka, A. Morimoto, and T. Kobayashi, Opt. Lett. **27**, 725 (2002).
8. J. D. Moody, B. J. MacGowan, J. E. Rothenberg, R. L. Berger, L. Divol, S. H. Glenzer, R. K. Kirkwood, E. A. Williams, and P. E. Young, Phys. Rev. Lett. **86**, 2810 (2001).
9. J. Fuchs, C. Labaune, S. Depierreux, H. A. Baldis, and A. Michard, Phys. Rev. Lett. **84**, 3089 (2000).
10. S. N. Dixit, M. D. Feit, M. D. Perry, and H. T. Powell, Opt. Lett. **21**, 1715 (1996).
11. D. H. Froula, L. Divol, R. L. Berger, R. A. London, N. B. Meezan, D. J. Strozzi, P. Neumayer, J. S. Ross, S. Stagnitto, L. J. Suter, and S. H. Glenzer, Phys. Rev. Lett. **101**, 115002 (2008).
12. D. H. Munro, S. N. Dixit, A. B. Langdon, and J. R. Murray, Appl. Opt. **43**, 6639 (2004).
13. J. E. Rothenberg, J. Appl. Phys. **87**, 3654 (2000).
14. Y. Zhang, W. Fan, J. Wang, X. Wang, X. Lu, D. Huang, S. Xu, Y. Zhang, M. Sun, Z. Jiao, S. Zhou, and X. Jiang, High Power Laser Sci. Eng. **12**, e9 (2024).

15. Y. Zhou, W. Fu, T. Zheng, T. Lin, L. Liu, X. Sun, Y. Geng, Y. Zhang, F. Fan, and S. Wen, Liquid Crystals **48**, 150 (2021).
16. Y. Wang, F. Wang, Y. Zhang, X. Huang, D. Hu, W. Zheng, R. Zhu, and X. Deng, Appl. Opt. **56**, 8087 (2017).
17. S. N. Dixit, D. Munro, J. R. Murray, M. Nostrand, P. J. Wegner, D. Froula, C. A. Haynam, and B. J. MacGowan, J. Phys. IV **133**, 717 (2006).
18. T. Z. Kosc, H. Huang, T. J. Kessler, and S. G. Demos, Opt. Express **30**, 12918 (2022).
19. H. Huang, T. Z. Kosc, T. J. Kessler, and S. G. Demos, High Power Laser Sci. Eng. **11**, e54 (2023).
20. S. S. Ban, Q. Wang, Z. J. Liu, C. Y. Zheng, and X. T. He, AIP Adv. **10**, 025123 (2020).
21. Z. J. Liu, B. Li, J. Xiang, L. H. Cao, C. Y. Zheng, and L. Hao, Plasma Phys. Control. Fusion **60**, 045008 (2018).
22. D. H. Edgell, P. B. Radha, J. Katz, A. Shvydky, D. Turnbull, and D. H. Froula, Phys. Rev. Lett. **127**, 075001 (2021).
23. D. H. Froula, I. V. Igumenshchev, D. T. Michel, D. H. Edgell, R. Follett, V. Yu. Glebov, V. N. Goncharov, J. Kwiatkowski, F. J. Marshall, P. B. Radha, W. Seka, C. Sorce, S. Stagnitto, C. Stoeckl, and T. C. Sangster, Phys. Rev. Lett. **108**, 125003 (2012).
24. A. Oudin, A. Debayle, C. Ruyer, and D. Bénisti, Phys. Rev. Lett. **127**, 265001 (2021).
25. R. A. Chipman, G. Young, and W. S. T. Lam, *Polarized Light and Optical Systems* (CRC Press, Boca Raton, 2018), p. 63.
26. M. Born and E. Wolf, *Principles of Optics: Electromagnetic Theory of Propagation, Interference and Diffraction of Light* (Pergamon Press, New York, 1980), p. 30.
27. B. Schaefer, E. Collett, R. Smyth, D. Barrett, and B. Fraher, Am. J. Phys. **75**, 163 (2015).
28. D. H. Goldstein and D. Goldstein, *Polarized Light* (Marcel Dekker, New York, 2003), p. 39.
29. A. M. Hansen, K. L. Nguyen, D. Turnbull, B. J. Albright, R. K. Follett, R. Huff, J. Katz, D. Mastrosimone, A. L. Milder, L. Yin, J. P. Palastro, and D. H. Froula, Phys. Rev. Lett. **126**, 075002 (2021).